



CrossMark  
click for updates

Cite this: *RSC Adv.*, 2015, 5, 24550

# Polyoxometalate-based layered nano-tubular arrays: facile fabrication and superior performance for catalysis†

Hongpeng Zhen,<sup>ab</sup> Xiaolin Li,<sup>b</sup> Lijuan Zhang,<sup>\*a</sup> Huan Lei,<sup>a</sup> Chao Yu,<sup>a</sup> Yunshan Zhou,<sup>\*b</sup> Sadaf ul Hassan,<sup>a</sup> Libo Qin<sup>a</sup> and Hafiz Muhammad Asif<sup>a</sup>

Keggin-type polyoxoanion  $\text{PW}_{12}\text{O}_{40}^{3-}$ -containing one-dimensional nano-tubular arrays, with the structure polyethylenimine/polystyrenesulfonate/(poly(allylammonium)/polystyrenesulfonate)<sub>5</sub>(poly(allylammonium)/ $\text{PW}_{12}\text{O}_{40}^{3-}$ )<sub>8</sub>, were fabricated as a prototype using a layer-by-layer deposition technique in porous anodic aluminum oxide and polycarbonate templates with a pore diameter of 200 nm, and characterized by IR, UV-vis and SEM. The resulting nano-tubes have a uniform diameter of  $180 \pm 20$  nm and a uniform wall thickness of  $30 \pm 5$  nm. These arrays have shown superior performance in the UV light irradiated photo-degradation of Rhodamine B (selected as a representative dye) under mild conditions with respect to both the catalytic efficiency and operating convenience due to the confinement within the nano-tubes both in the latitudinal and radial direction. Remarkably, the catalytic activity of the nano-tubular arrays could be recovered by means of simple immersion in the polyoxoanion solution when the catalytic reactivity became reduced, which is vital in view of practical applications. The total organic carbon content changes and GC-MS measurements were conducted to identify the degradation products. The hydroxyl radical mechanism was found to be adopted by the photo-degradation reaction.

Received 21st January 2015  
Accepted 23rd February 2015

DOI: 10.1039/c5ra01247c

[www.rsc.org/advances](http://www.rsc.org/advances)

## Introduction

Polyoxometalates (POMs) are a class of discrete transition metal anionic clusters with abundant compositions, structures and versatile properties leading to their successful application in various fields.<sup>1-3</sup> Among the important/potential applications, the catalytic activities of POMs are the most fascinating feature and they are outstanding for use in homo-/heterogeneous acid or redox catalyses<sup>4-8</sup> with advantages such as photo-/thermal stability,<sup>9,10</sup> non-toxicity,<sup>11</sup> low cost and environmentally friendly behavior.<sup>12</sup> However, most POMs are highly-soluble in aqueous solution and form a homogeneous catalyst which is often inconvenient for industrial purposes.<sup>13,14</sup> In contrast, heterogeneous catalysis is easier to run and separate, yielding a sustainable catalytic process. Many efforts have been made towards the heterogenization of homogeneous POM-based catalysts such as the syntheses of heterogeneous catalysts by combining POMs with counter cations such as  $\text{K}^+$ ,  $\text{Cs}^+$  and

$\text{NH}_4^+$ ,<sup>15-17</sup> or formation of nanoparticles and/or preparation of films by coating POMs onto inorganic/organic composites such as  $\text{TiO}_2$ ,  $\text{SiO}_2$ , activated carbon or organic polymer.<sup>18-21</sup> However, the exploration of new approaches to synthesise POM catalysts that can be separated more conveniently from reaction systems and have a more convenient recycling process as well as an enhanced superior catalytic performance still remains challenging.

Inspired by the continuing great success of nanotubular materials in various fields,<sup>22,23</sup> incorporating polyoxometalates into nano-tubular arrays may be expected to overcome limitations *i.e.*, small surface area<sup>24</sup> and difficulty in recycling and reuse due to water solubility,<sup>13</sup> as well as to realize upgraded catalytic activity because of the specific characteristics such as the nanotubular shape with controllable wall thickness and aperture, high specific surface area exhibiting more active sites, confinement both in the latitudinal and radial direction within the nano-tubes and the possible synergistic and coupling effects of arrays. In this work, we report the fabrication and characterization of nano-tubular arrays based on the well-known  $\alpha$ -Keggin-type  $\text{H}_3\text{PW}_{12}\text{O}_{40}$ , which is selected as a representative due to its superior performance as a catalyst<sup>15,25-33</sup> (1882 references were found containing the concept “tungstophosphoric acid catalysis” in the SciFinder database on Jan 16, 2015). The nano-tubular arrays showed an excellent performance as a photo-catalyst to degrade RhB (difficult to degrade completely

<sup>a</sup>State Key Laboratory of Chemical Resource Engineering, Beijing University of Chemical Technology, Beijing 100029, China. E-mail: zhouys@mail.buct.edu.cn; ljzhang@mail.buct.edu.cn; Tel: +86-10-64414640

<sup>b</sup>College of Materials Science and Engineering, Beijing University of Chemical Technology, Beijing 100029, China

† Electronic supplementary information (ESI) available: Fig. S1–S9 and Table S1. DOI: 10.1039/c5ra01247c

by conventional methods and also suspected to be carcinogenic) under UV-vis light irradiation. Importantly, the catalytic activity of the POM nano-tubular arrays can be renewed by simple immersion in a  $\text{H}_3\text{PW}_{12}\text{O}_{40}$ -containing solution when the catalytic reactivity is reduced after recycling many times, which is very important in view of practical applications.

## Experimental

Polyethylenimine (PEI, MW 50 000) and sodium polystyrenesulfonate (PSS, MW 70 000) were purchased from Aldrich. Poly(allylammonium chloride) (PAH, MW 70 000) was purchased from Alfa Aesar. The solution of PEI ( $10 \text{ mg mL}^{-1}$ ), PSS ( $2 \text{ mg mL}^{-1}$ ) and PAH ( $1 \text{ mg mL}^{-1}$ ), each containing  $0.1 \text{ mol L}^{-1}$  of NaCl to enhance the ionic strength, was prepared at pH 1.5 adjusted by dilute HCl.  $\text{H}_3\text{PW}_{12}\text{O}_{40} \cdot n\text{H}_2\text{O}$  and RhB were purchased from Sinopharm Chemical Reagent Beijing Co., Ltd. All reagents used in this work were of analytical grade and used as received. Deionized water was used throughout the experiments. Porous anodic aluminium oxide membrane (AAO template: diameter 25 mm, pore diameter 200 nm, average film thickness  $60 \mu\text{m}$ ) and nucleoporetrack-etched polycarbonate membranes (PC template: diameter 25 mm, pore diameter 200 nm, average film thickness  $20 \mu\text{m}$ ) were purchased from Whatman corp. The structures of the reactants used are shown in Fig. 1.

### Instruments and techniques of measurement

The FT-IR spectra were recorded on a MAGNA-IR 750 (Nicolet) spectrophotometer with KBr pellets in the range of  $400\text{--}4000 \text{ cm}^{-1}$ . Light intensity was recorded by a radiometer FZ-A (the photoelectric instrument factory of Beijing Normal University, China). Scanning electron microscopy (SEM) and energy dispersive X-ray spectroscopy were carried out on a Zeiss Supra 55 scanning electron microscope. The UV-vis spectra were recorded on a SHIMADZU UV-2550 spectrometer. The photo-reaction was conducted under a 250 W high-pressure mercury lamp with a light intensity of  $22 \text{ mW cm}^{-2}$ . GC/MS analyses were carried out on a Shimadzu GC/MS QP2010 system

equipped with a DB-5 MS capillary column ( $30 \text{ mm} \times 0.25 \text{ mm}$ ). The temperature program of the column was set as follows: at  $60 \text{ }^\circ\text{C}$ , hold time = 1 min; from 60 to  $250 \text{ }^\circ\text{C}$ , rate  $20 \text{ }^\circ\text{C min}^{-1}$ . The TOC measurement was performed on a Shimadzu TOC-5000A analyser. Photoluminescence spectra were obtained on a Hitachi F-7000 fluorescence spectrophotometer with an emission slit of 5 nm using a 150 W xenon lamp as the light source. The millipore filter setup for preparing the nano-tubular array and carrying out the photo-catalysis reaction was purchased from Auto science Co., Ltd ( $40 \text{ mL}$  in volume and  $25 \text{ mm}$  in diameter) (Fig. S1†).

### Preparation of $\text{PEI/PSS}/(\text{PAH/PSS})_3(\text{PAH/PW}_{12}\text{O}_{40}^{3-})_8$ nano-tubular arrays within porous templates

The AAO template was kept on the millipore filter (Fig. S1†) and the pressure was adjusted to  $0.020 \text{ MPa}$  by a buffering device to prevent it from breaking. Firstly,  $20 \text{ mL}$  deionized water was flowed through the template from each side under low pressure conditions, then a  $20 \text{ mL}$  PEI solution was flowed through the template from each side. Subsequently, the template was immersed into deionized water for 10 min and then washed with  $10 \text{ mL}$  deionized water. Similarly, PSS and PAH were alternately adsorbed onto the inner wall of the porous template forming a precursor film with the structure  $(\text{PEI/PSS})/(\text{PAH/PSS})_3$ . Then, PAH and  $\text{PW}_{12}\text{O}_{40}^{3-}$  were alternately adsorbed onto the precursor film from a PAH and a  $\text{H}_3\text{PW}_{12}\text{O}_{40}$  solution ( $10^{-3} \text{ mol L}^{-1}$ ), respectively, resulting in the formation of layered nano-tubular arrays with the structure  $\text{PEI/PSS}/(\text{PAH/PSS})_3(\text{PAH/PW}_{12}\text{O}_{40}^{3-})_8$  within the pores of the AAO template (denoted  $\text{PW}_{12}\text{-AAO}$ ). All the preparation processes were performed under ambient conditions. The same procedure was performed when a PC template was used, resulting in the formation of nano-tubular arrays with the structure  $\text{PEI/PSS}/(\text{PAH/PSS})_3(\text{PAH/PW}_{12}\text{O}_{40}^{3-})_8$  within the pore of the PC template (denoted  $\text{PW}_{12}\text{-PC}$ ). The fabrication process of POM/polyelectrolyte nano-tubular arrays through LBL coating and the sequential release of nano-tubes are shown in Fig. 2. Release and collection of the nano-tubes from the PC template for characterization was carried out by dissolving the PC template in chloroform followed by centrifugation of the solution. The

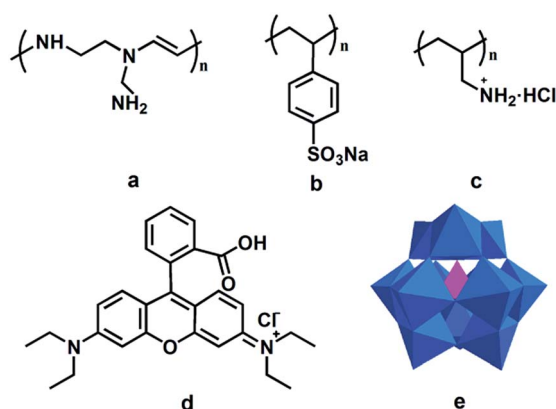


Fig. 1 Structures of the polyelectrolyte PEI (a), PSS (b), PAH (c), dye RhB (d), and the anion  $\text{PW}_{12}\text{O}_{40}^{3-}$  (e).

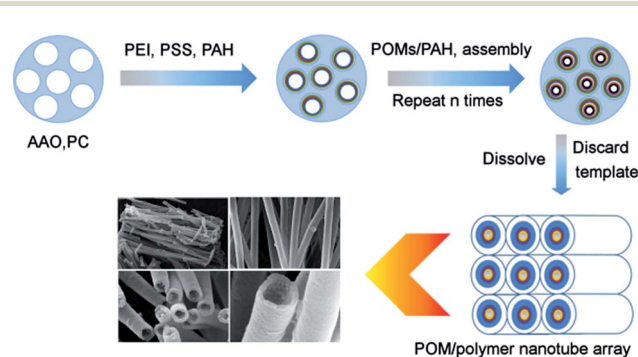


Fig. 2 Schematic diagram illustrating the fabrication process of  $\text{PEI/PSS}/(\text{PAH/PSS})_3(\text{PAH/PW}_{12}\text{O}_{40}^{3-})_8$  nano-tubular arrays within the PC/AAO template through the LBL coating method and release of the nano-tubes from the template for characterization.

method used for release and collection of the nano-tubes from the AAO template is given in the ESI.†

### Preparation of PEI/PSS/(PAH/PSS)<sub>3</sub>(PAH/PW<sub>12</sub>O<sub>40</sub><sup>3-</sup>)<sub>n</sub> multi-layered nanofilms on a substrate

A quartz plate was immersed into a fresh piranha solution (conc. H<sub>2</sub>SO<sub>4</sub>/30% H<sub>2</sub>O<sub>2</sub> = 7 : 3 (v/v)) at 80 °C for 1 h, then rinsed with a copious amount of deionized water and dried in a nitrogen atmosphere. After immersion in PEI and PSS, then alternately in PAH and PSS for three cycles and finally alternately in PAH and H<sub>3</sub>PW<sub>12</sub>O<sub>40</sub> (10<sup>-3</sup> mol L<sup>-1</sup>) each for 20 min, the coated quartz was characterized by UV-vis in order to monitor and determine the growth of (PAH/PW<sub>12</sub>O<sub>40</sub><sup>3-</sup>) bilayers.

### Photo-degradation of RhB by PEI/PSS/(PAH/PSS)<sub>3</sub>(PAH/PW<sub>12</sub>O<sub>40</sub><sup>3-</sup>)<sub>8</sub> nano-tubular arrays

For the photo-catalytic reaction, a high-pressure mercury lamp was used as the light source. 40 mL of RhB solution (2 mg RhB per liter of solution) was filtered through the PW<sub>12</sub>-AAO and PW<sub>12</sub>-PC catalyst, respectively, which were placed on the millipore filter (Fig. S1†). The entire degradation process was carried out under ambient conditions. The characteristic absorbance changes at λ<sub>max</sub> = 554 nm of RhB were monitored and the decoloration efficiency (DE) was calculated by the equation: DE = [(A<sub>0</sub> - A<sub>t</sub>)/A<sub>0</sub>] × 100%, where A<sub>0</sub> stands for the absorbance before the reaction, and A<sub>t</sub> stands for the absorbance at given filtration times.

## Results and discussion

### Fabrication and characterization of PEI/PSS/(PAH/PSS)<sub>3</sub>(PAH/PW<sub>12</sub>)<sub>8</sub> nano-tubular arrays

Despite the so-called layer-by-layer (LBL) technique (*viz.*, immersing a porous template such as AAO and PC alternately into different reactant-containing solutions) having been commonly adopted for preparing polyelectrolyte-involving nano-tubes, this method usually suffers from an unavoidable drawback, *viz.*, the entrance of nano-/micro-sized pores of the template are easily blocked due to the strong interaction between the charged polyelectrolyte and the oppositely charged template surface, which prevents the polyelectrolyte molecules and other reactants from entering the pores and anchoring to the inner template walls.<sup>34</sup> Consequently, the desired nano-/microtubes cannot be formed inside the pores of the template in the process of alternate immersion.

In our present work, the blockage problem has been effectively solved by using a reduced pressure filtration process, where the pressurized flow of solutions of alternately charged polyelectrolytes/polyoxoanions and the neutral washing steps between them results in the LBL deposition of a PEI/PSS/(PAH/PSS)<sub>3</sub>(PAH/PW<sub>12</sub>)<sub>8</sub> multilayer on the inner walls of the template.

UV-vis spectrum measurement is an effective method to monitor the growth of a film which is formed by the LBL technique. Since it is very difficult to directly monitor the growth of each bilayer of (PAH/PW<sub>12</sub>) in the nanopores of the template,

the growth of a POM film (PAH/PW<sub>12</sub>O<sub>40</sub><sup>3-</sup>)<sub>n</sub> on a quartz plate was monitored instead.<sup>35</sup> It was found that while the characteristic absorption<sup>35,36</sup> of the Keggin-type PW<sub>12</sub> appearing at 266 nm attributed to the W ← O<sub>b,c</sub> charge transition does not change in position during the whole deposition process, the absorbance intensity increases linearly with the increasing number of bilayers, (PAH/PW<sub>12</sub>O<sub>40</sub><sup>3-</sup>)<sub>n</sub> (n = 1–8) (Fig. 3). This not only confirms the alternate deposition of negatively charged PW<sub>12</sub>O<sub>40</sub><sup>3-</sup> anions and positively charged PAH but also demonstrates that the thickness of the films is precisely controllable. Though this result is obtained from a flat surface and may not be directly extended to a cylindrical type substrate, however, we expect that the same linear relationship exists for the growth of (PAH/PW<sub>12</sub>O<sub>40</sub><sup>3-</sup>)<sub>n</sub> nano-tubes.

The SEM images of the PEI/PSS/(PAH/PSS)<sub>3</sub>(PAH/PW<sub>12</sub>O<sub>40</sub><sup>3-</sup>)<sub>8</sub> nano-tubes released from the PC template (Fig. 4) show that the tubes have a uniform diameter of 180 ± 20 nm and a uniform wall thickness which reaches 30 ± 5 nm. The average thickness of each (PAH/PW<sub>12</sub>O<sub>40</sub><sup>3-</sup>) bilayer is roughly calculated to be *ca.* 2 nm (Fig. 4b). The SEM images of nano-tubes released from AAO template (Fig. S2†) illustrates tubular structures with uniform diameter of 180 nm ± 20 nm and a wall thickness of 20 ± 5 nm which is a little thinner than nano-tubes released from PC template because of partial dissolution during release process in phosphoric acid (ESI†).

The FT-IR spectra of PEI/PSS/(PAH/PSS)<sub>3</sub>(PAH/PW<sub>12</sub>O<sub>40</sub><sup>3-</sup>)<sub>8</sub> nano-tubes (Fig. S3†) show the four characteristic peaks<sup>15,16,35,36</sup> of α-Keggin-type PW<sub>12</sub>O<sub>40</sub><sup>3-</sup>: P–O bond in PO<sub>4</sub> (ν<sub>as</sub> = 1083 cm<sup>-1</sup>), W–O<sub>b</sub>–W bond (ν<sub>as</sub> = 890 cm<sup>-1</sup>), W–O<sub>c</sub>–W bond (ν<sub>as</sub> = 800 cm<sup>-1</sup>) (O<sub>b</sub> is the oxygen atom between the two different W<sub>3</sub>O<sub>13</sub> groups, O<sub>c</sub> is the oxygen atom in the same W<sub>3</sub>O<sub>13</sub> group) and W=O<sub>d</sub> bonds (ν<sub>as</sub> = 952 cm<sup>-1</sup>). The red/blue shift of peaks compared to the parent PW<sub>12</sub>O<sub>40</sub><sup>3-</sup> can be attributed to the strong attraction between negatively charged PW<sub>12</sub>O<sub>40</sub><sup>3-</sup> and positively charged PAH. The semi-quantitative EDX analyses (Fig. S4†) show that the P/W atom ratio of the nano-tubes released from the templates is 1.13 : 10.52, which is relatively close to the ratio of PW<sub>12</sub>O<sub>40</sub><sup>3-</sup> (P/W = 1 : 12). The above analyses further confirm that the PW<sub>12</sub>O<sub>40</sub><sup>3-</sup> structure remains intact in the tubular arrays.

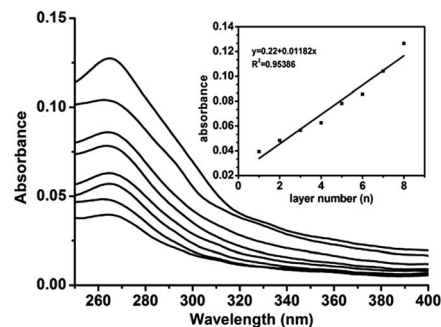


Fig. 3 The UV-vis spectra of PEI/PSS/(PAH/PSS)<sub>3</sub>(PAH/PW<sub>12</sub>O<sub>40</sub><sup>3-</sup>)<sub>n</sub> (n = 1–8) multilayered films. The inset shows the linear relationship between absorbance intensity at 266 nm and the number of (PAH/PW<sub>12</sub>O<sub>40</sub><sup>3-</sup>) bilayers.

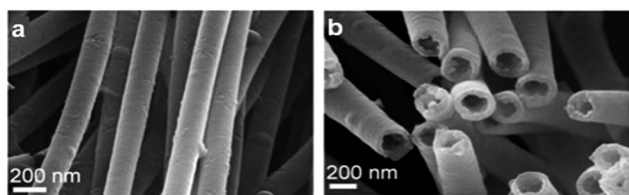


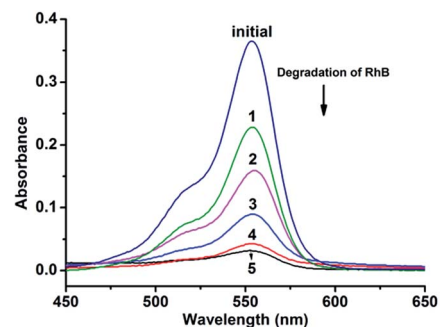
Fig. 4 The SEM images of PEI/PSS/(PAH/PSS)<sub>3</sub>(PAH/PW<sub>12</sub>O<sub>40</sub><sup>3-</sup>)<sub>8</sub> nano-tubes released from the PC template: (a) the side view of the nano-tubes; (b) the cross-section view of the nano-tubes.

### Photo-degradation of RhB solution by PEI/PSS/(PAH/PSS)<sub>3</sub>(PAH/PW<sub>12</sub>O<sub>40</sub><sup>3-</sup>)<sub>8</sub> nano-tubular arrays

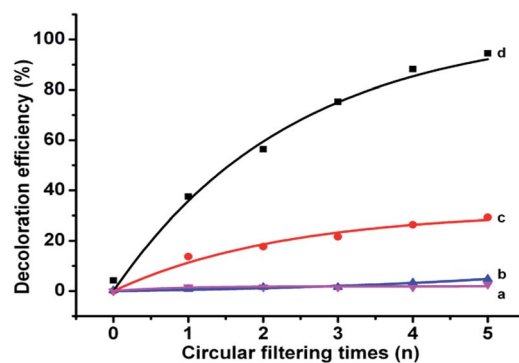
In the preliminary experiments, a PW<sub>12</sub>-AAO was first immersed into the dye solution for 0.5 h to ensure adsorption-desorption equilibrium between the dye and the catalyst under dark conditions in order to avoid the effect of adsorption of the dye before all the measurements.<sup>28</sup> Initially, the influence of the light source on the degradation efficiency was discussed. Four types of experiments were conducted: (1) under daylight irradiation with bare AAO, (2) under UV light irradiation with bare AAO, (3) under daylight irradiation with the PW<sub>12</sub>-AAO and (4) under UV light irradiation with the PW<sub>12</sub>-AAO. Under each of the four conditions, 40 mL of RhB solution was filtered 5 times circularly through a bare AAO template and a PW<sub>12</sub>-AAO. The results showed that RhB was more remarkably degraded (Fig. 5, Table S1<sup>†</sup>) under UV irradiation in the presence of the nano-tubular arrays as compared to the other conditions (Fig. S5<sup>†</sup>). The decoloration efficiency reached a maximum of 94.5% after circular filtration 5 times under UV light irradiation with the PW<sub>12</sub>-AAO catalyst at pH 5. The results indicated that UV irradiation and the nano-tubular array catalyst are compulsory for the degradation of RhB.

As shown in Fig. 6 and Fig. S6,<sup>†</sup> the photo-degradation efficiency varies at different pH values of RhB solution (pH = 3.0, 4.0, 5.0, and 6.0) under the optimal conditions, *viz.*, UV light irradiation with PW<sub>12</sub>-AAO (Table 1). The results show that PEI/PSS/(PAH/PSS)<sub>3</sub>(PAH/PW<sub>12</sub>O<sub>40</sub><sup>3-</sup>)<sub>8</sub> nano-tubular arrays have a higher photo-catalytic activity at a lower pH value of the reaction system (decoloration efficiency rises from 79.6% (pH = 6.0) to 97.8% (pH = 3.0)), which suggests that the acidic condition is favorable to the degradation of RhB molecules in the presence of the catalyst. It should be noted that the observation of effect of the pH on photocatalytic RhB degradation is analogous to those previously reported.<sup>31</sup> However, when the pH value decreases below 2.5, the acid-base equilibrium of RhB in solution, H<sub>2</sub>RhB<sup>2+</sup> ↔ HRhB<sup>+</sup> ↔ RhB, will change and RhB may combine with more protons to form the protonated structure H<sub>2</sub>RhB<sup>2+</sup>, which causes a blue shift<sup>37</sup> of the peak from 554 nm for RhB to 495 nm for H<sub>2</sub>RhB<sup>2+</sup> and consequently it gets difficult to monitor the catalytic efficiency at 554 nm using UV-vis spectral measurements. Therefore, conditions at pH < 2.5 are not considered in this study.

The above results clearly demonstrate that the new nano-tubular array system shows high-efficient catalytic ability



(a)



(b)

Fig. 5 UV-vis absorption spectral changes of RhB vs. circular filtering times at pH 5 under UV light with PW<sub>12</sub>-AAO (where the repeated filtration process of filtered RhB solution through the catalyst is called circular filtering). The arrow mark shows the degradation of the RhB with increasing number of circular filtering (initial, original RhB solution; 1, first time filtering; 2, second time filtering; 3, third time filtering; 4, fourth time filtering; and 5, fifth time filtering) (a) and the degradation effect of RhB under four different conditions: daylight with bare AAO (line a), UV light with bare AAO (line b), daylight with PW<sub>12</sub>-AAO (line c) and UV light with PW<sub>12</sub>-AAO (line d) (b).

under the optimal conditions, *viz.*, UV light irradiation and pH = 3. In addition, since the AAO template has better parallel array morphology, larger pore density and greater thickness (Fig. S2c and d<sup>†</sup>) than the PC template (Fig. S7a<sup>†</sup>), the total

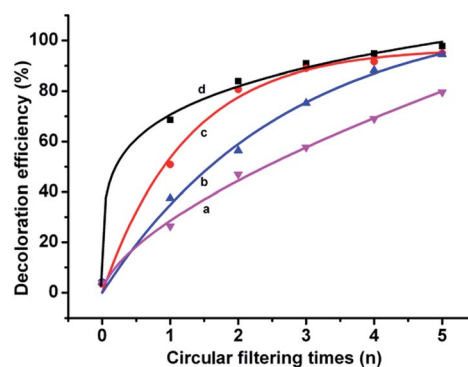


Fig. 6 Effect of pH on photo-degradation of RhB (line a, pH 6.0; line b, pH 5.0; line c, pH 4.0 and line d, pH 3.0) vs. circular filtering times for RhB solution with PW<sub>12</sub>-AAO under UV light.



**Table 1** The effect of pH values on RhB degradation under UV light irradiation with PW<sub>12</sub>-AAO

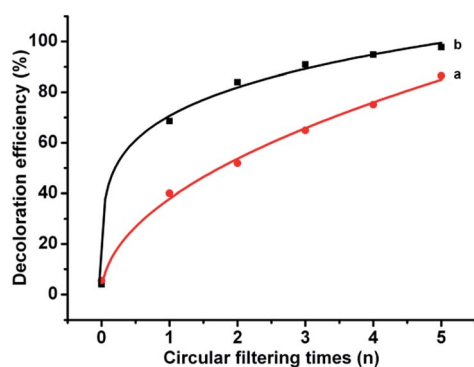
Group	pH	Circulation times	Degradation efficiency (%)
1	6.0	5	79.6
2	5.0	5	94.5
3	4.0	5	95.0
4	3.0	5	97.8

number of nano-tubes and catalyst loading capacity within the AAO template is subsequently larger than that within the PC template, and the nano-tubular arrays obtained from AAO are better than those from PC in terms of both quantity and regularity. Consequently, much better photo-catalytic decoloration results were obtained when PW<sub>12</sub>-AAO was used (decoloration efficiency DE = 98%) (Fig. 7 and S8†) as compared with PW<sub>12</sub>-PC (decoloration efficiency DE = 91%) under the same optimal conditions.

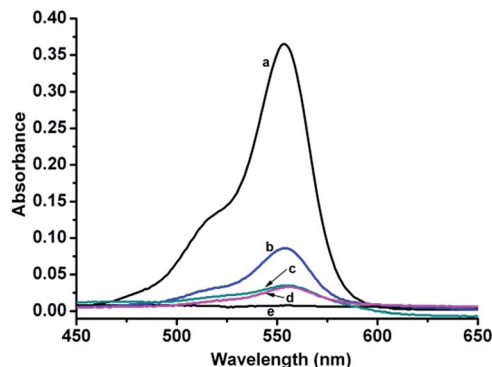
Interestingly, it was observed that when 5 PW<sub>12</sub>-AAOs and 5 PW<sub>12</sub>-PCs were overlapped respectively and used once at the optimal catalytic conditions, the photo-catalytic decoloration efficiency (DE = 91% for 5 PW<sub>12</sub>-AAOs, 77% for 5 PW<sub>12</sub>-PCs) was a little bit weaker than that for filtering 5 times using a single PW<sub>12</sub>-AAO (DE = 98%) and a single PW<sub>12</sub>-PC (DE = 90%) (Fig. 8), respectively. This result could be tentatively attributed to the fact that the middle nanotubular arrays cannot be well irradiated by UV light when five PW<sub>12</sub>-AAOs/PW<sub>12</sub>-PCs overlap tightly together. Despite this moderate decrease in photo-degradation efficiency, remarkable convenience is achieved when 5 overlapped PW<sub>12</sub>-AAOs and 5 overlapped PW<sub>12</sub>-PCs were used for one circular filtration as compared to using single PW<sub>12</sub>-AAO and single PW<sub>12</sub>-PC and filtering 5 times.

#### Total organic carbon (TOC) measurement in the degradation of RhB and identification of the final products

Fig. 9 shows the TOC changes during photo-degradation of RhB with circular filtering times with a PW<sub>12</sub>-AAO under the optimal



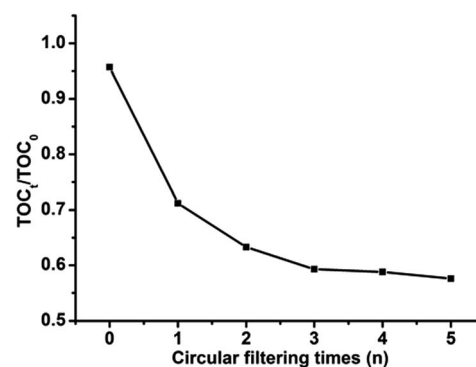
**Fig. 7** The comparison of RhB decoloration efficiency with PW<sub>12</sub>-PC (line a) and with PW<sub>12</sub>-AAO (line b) after 5 circular filtering times under the optimal conditions.



**Fig. 8** UV-vis absorption spectral changes of RhB by filtering once through 5 overlapped PW<sub>12</sub>-PCs (line b) and 5 overlapped PW<sub>12</sub>-AAOs (line c), and filtering 5 circular times through one PW<sub>12</sub>-AAO (line e) and one PW<sub>12</sub>-PC (line d) at the optimal catalytic conditions. Line a is the UV-vis spectrum of the original RhB solution.


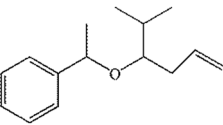
conditions. Prior to degradation, the PW<sub>12</sub>-AAO was immersed in the dye solution (40 mL, 2 mg L<sup>-1</sup>) for 0.5 h in the dark. The maximum TOC removal of RhB was observed to be 42.6% (from 1.77 to 1.02 ppm) at the point when the solution was almost decolorized after 5 circular filtering times. Therefore, it can be concluded that around half of the dye was mineralized into CO<sub>2</sub> during the degradation process. However, CO<sub>2</sub> was not the only product as some other organic products were also generated. Under the same conditions, the maximum TOC removal of RhB was 37.7% with PW<sub>12</sub>-PC used as the photo-catalyst, which is a little inferior to PW<sub>12</sub>-AAO.

A GC/MS technique was used to analyse the final products of RhB degradation. The listed products in Table 2 are the main parts of the RhB framework besides CO<sub>2</sub> while the other products with greatly lower intensities are neglected. From the above results, it can be concluded that the conjugated xanthene structure of RhB was partially split up during the degradation reaction<sup>25,26,28,29,31,37,38</sup> in the presence of PEI/PSS/(PAH/PSS)<sub>3</sub>(PAH/PW<sub>12</sub>)<sub>8</sub> nanotubular arrays under the UV light. The relative amount of each degradation product was calculated according to the TOC changes (Table 2).



**Fig. 9** TOC changes during photo-degradation of RhB versus circular filtering times with PW<sub>12</sub>-AAO as the catalyst under the optimal conditions.

Table 2 Final major products of the photo-degradation of RhB and their respective amounts detected by GC/MS

Retention time (min)	Detected product	Relative amount
1.0		0.18
1.25		0.06
5.2	CH <sub>3</sub> (CH <sub>2</sub> ) <sub>6</sub> COOH	1.00

### Photo-catalysis mechanism study

Photo-degradation of RhB has been performed by PW<sub>12</sub>O<sub>40</sub><sup>3-</sup> under various conditions, *e.g.*, sunlight with H<sub>2</sub>O<sub>2</sub>,<sup>15,25,26</sup> sunlight<sup>27–30</sup> and UV light.<sup>31,33</sup> Generally, it is accepted that under UV irradiation, the excited POM molecule induces an electron transition from the highest occupied molecular orbital (HOMO) to the lowest unoccupied molecular orbital (LUMO). The excited state of the POM (POM\*) can generate ·OH radicals in a water solution, which are extremely powerful oxidizing agents to oxidize organic substrates. While the reduced POM (POM<sup>-</sup>) produced from the POM\* by abstracting an electron from electron-donating substances can deliver the electron to electron acceptors such as O<sub>2</sub>, metal ions and re-charge to oxidized POM.<sup>33,39</sup> Nevertheless, it needs to be confirmed whether or not the photo-catalytic processes in our work adopt a similar hydroxyl radical mechanism. It is known that hydroxyl radicals can be detected by the photoluminescence (PL) technique using terephthalic acid (TA) as a probe molecule since the hydroxyl radicals can readily react with TA to produce a highly fluorescent product 2-hydroxyterephthalic acid.<sup>33</sup> This method is based on the PL signal of 2-hydroxyterephthalic acid at 425 nm. Moreover, the PL intensity of 2-hydroxyterephthalic acid is proportional to the concentration of ·OH radicals which are produced from POM catalysis. So, a similar procedure for the measurement of photo-catalytic activity was carried out whereby just the RhB aqueous solution was replaced by the 5 × 10<sup>-4</sup> M TA aqueous solution (TA was dissolved in 2 × 10<sup>-3</sup> M NaOH solution). A gradual increase in PL intensity at about 425 nm (excited by 315 nm UV-light) is observed with an increasing irradiation time for the nano-tubes released from PC templates (Fig. 10), while no PL increase is observed in the absence of UV light or the nano-tubes. This suggests that the fluorescence is due to the chemical reactions between terephthalic acid and ·OH produced at the catalyst/water interface under UV illumination.<sup>33</sup> Further observation indicates that the PL intensity change is not linear with the irradiation time. This can be ascribed to the fact that the PW<sub>12</sub> catalyst is not stable in such high basic conditions and can be decomposed gradually.

Though it is difficult to demonstrate quantitatively how the microstructure has helped the catalysis, it can be said that due to the high specific surface area exhibiting more active sites and

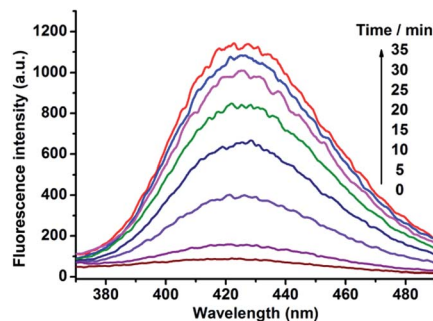


Fig. 10 Photoluminescence spectral changes ( $\lambda_{\max} = 425$  nm) versus UV light irradiation time on the nano-tubes released from PC templates in a 5 × 10<sup>-4</sup> M basic solution of terephthalic acid (excitation light  $\lambda = 315$  nm, voltage = 500 V, EX-Slit = 10 nm, EM-Slit = 10 nm).

the fact that the ·OH radicals are produced at the catalyst/water interface under UV light illumination, the density of ·OH radicals becomes greater and greater in the direction from the center of the nano-tubes to the inner surface of the nano-tubes. Meanwhile, the confinement both in the latitudinal and radial direction within the arrays forces the RhB molecules to flow through the nano-tubes leading to more opportunities to access the produced reactive ·OH radicals which can decompose RhB into different species (Table 2) besides CO<sub>2</sub>. As a result, the nano-tubular arrays present unique capabilities.

### Renewable catalytic activity of the PEI/PSS/(PAH/PSS)<sub>3</sub>(PAH/PW<sub>12</sub>)<sub>8</sub> nano-tubular arrays

Under the obtained optimal conditions, renewal and reuse of the nano-tubular arrays was tested. In the experiment, 5 overlapped PW<sub>12</sub>-AAOs and 5 overlapped PW<sub>12</sub>-PCs were used as catalysts for filtering a RhB solution, respectively. It was observed that the catalytic activity of the nano-tubular arrays in both AAO and PC faded after successive reuse (Fig. S9†). This could be due to the loss of the POMs on the inner surface of the

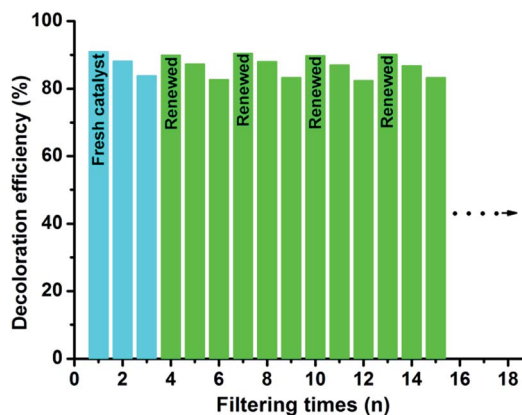


Fig. 11 Catalytic activity of fresh catalyst (5 overlapped PW<sub>12</sub>-PCs) (cyan column) and the renewed catalysts (green column). Each renewal process was conducted after the catalyst had been used to photo-degrade fresh RhB solution three times.

nano-tubes indicating that POMs leached into the solution can not carry out catalysis as effectively as those within the nano-tubular arrays because of the absence of confinement both in the latitudinal and radial direction. Importantly, the catalytic activity of the POM nano-tubular arrays can be fully renewed by simple immersion in a  $\text{H}_3\text{PW}_{12}\text{O}_{40}$ -containing mother solution (Fig. 11) and can be reused as efficiently as a fresh catalyst. Obviously, this is very important in view of practical applications.

## Conclusion

In summary, we successfully prepared PEI/PSS/(PAH/PSS)<sub>3</sub>-(PAH/PW<sub>12</sub>O<sub>40</sub><sup>3-</sup>)<sub>8</sub> nano-tubular arrays in the porous templates, AAO and PC, using the LBL method as a prototype, which not only allowed the precise structural design (controllable wall thickness and aperture) and control of the geometrical features (linear growth and smooth surface) but also solved the template pore blocking problem by a combination of the reduced pressure filtration process and neutral washing steps. The fabricated POM nano-tubular arrays exhibited excellent effects on the photo-degradation of RhB under mild conditions and the catalytic activity of the POM nano-tubular arrays can be fully renewed by simple immersion in a  $\text{H}_3\text{PW}_{12}\text{O}_{40}$ -containing mother solution when the catalytic reactivity fades. From an economic and environmental viewpoint, efforts to get POMs anchored onto the inner tube surface by relatively strong covalent bonds were also undertaken to avoid leaching of POMs. Given the large number of polyoxometalates of various structures and properties reported in the literature, this work may provide new concepts for catalyst design and regeneration based on polyoxometalates with a nano-confinement effect, array effect and coupling effect, which show extensive potential/practical applications for the design of reactors with specific sizes for specific reaction systems.

## Acknowledgements

The financial support of the Natural Science Foundation of China, PCSIRT (no. IRT1205), the Fundamental Research Funds for the Central Universities (YS1406) and Beijing Engineering Center for Hierarchical Catalysts is greatly acknowledged. Prof. Xue Duan of Beijing University of Chemical Technology is greatly acknowledged for his kind support.

## Notes and references

- C. L. Hill, A themed issue on polyoxometalate chemistry, *Chem. Rev.*, 1998, **98**, 1–387.
- P. Kögerler, B. Tsukerblat and A. Müller, *Dalton Trans.*, 2010, **39**, 21–36.
- L. Cronin and A. Müller, A themed issue on polyoxometalate chemistry, *Chem. Soc. Rev.*, 2012, **41**, 9799–10106; D. Long and L. Cronin, A themed issue entitled polyoxometalate cluster science, *Chem. Soc. Rev.*, 2012, **41**, 7325–7633.
- M. Misono and N. Nojiri, *Appl. Catal.*, 1990, **64**, 1–30.
- C. L. Hill and C. M. Prosser-McCartha, *Coord. Chem. Rev.*, 1995, **143**, 407–455.
- T. Okada, K. Miyamoto, T. Sakai and S. Mishima, *ACS Catal.*, 2014, **4**(1), 73–78.
- C. W. Hu, M. Hashimoto, T. Okuhara and M. Misono, *J. Catal.*, 1993, **143**, 437–438.
- A. Hiskia, A. Mylonas and E. Papaconstantinou, *Chem. Soc. Rev.*, 2001, **30**, 62–69.
- M. Misono, *Chem. Commun.*, 2001, 1141–1152.
- M. A. Fox, R. Cardona and E. Gaillard, *J. Am. Chem. Soc.*, 1987, **109**, 6347–6354.
- C. L. Hill and D. A. Bouchard, *J. Am. Chem. Soc.*, 1985, **107**, 5148–5157.
- R. Noyori, M. Aoki and K. Sato, *Chem. Commun.*, 2003, 1977–1986.
- M. T. Pope, *Heteropoly and Isopoly-Oxometalates*, Springer-Verlag, Berlin, 1983.
- D. A. Friesen, L. Morello, J. V. Headley and C. H. Langford, *J. Photochem. Photobiol., A*, 2000, **133**, 213–220.
- C. C. Chen, Q. Wang, P. X. Lei, W. J. Song, W. H. Ma and J. C. Zhao, *Environ. Sci. Technol.*, 2006, **40**, 3965–3970.
- T. Ito, K. Inumaru and M. Misono, *J. Phys. Chem. B*, 1997, **101**, 9958–9963.
- J. Haber, K. Pamin, L. Matachowski, B. Napruszewska and J. Poltowicz, *J. Catal.*, 2002, **207**, 296–306.
- C. Ramesh Kumar, N. Rambabu, K. C. Maheria, A. K. Dalai and N. Lingaiah, *Appl. Catal., A*, 2014, **485**, 74–83.
- A. Maldotti, A. Molinari and F. Bigi, *J. Catal.*, 2008, **253**, 312–317.
- J. D. Torres, E. A. Faria, J. R. DeSouza and A. G. S. Prado, *J. Photochem. Photobiol., A*, 2006, **182**, 202–206.
- C. J. Yang, L. H. Tian, L. Q. Ye, T. Y. Peng, K. J. Deng and L. Zan, *J. Appl. Polym. Sci.*, 2011, **120**, 2048–2053.
- S. Iijima, *Nature*, 1991, **354**, 56–58.
- Y. N. Xia, P. D. Pang, Y. G. Sun, Y. Y. Wu, B. Mayers, B. Gates, Y. D. Yin, F. Kim and H. Q. Yan, *Adv. Mater.*, 2003, **15**, 353–389.
- C. Marchena, R. A. Frenzel, S. Gomez, L. B. Pierella and L. S. Pizzio, *Appl. Catal., B*, 2013, **130–131**, 187–196.
- S. Y. Gao, R. Cao, J. Lv, G. L. Li, Y. F. Li and H. X. Yang, *J. Mater. Chem.*, 2009, **19**, 4157–4163.
- Y. You, S. Y. Gao, Z. Yang, M. N. Cao and R. Cao, *J. Colloid Interface Sci.*, 2012, **365**, 198–203.
- C. C. Chen, Q. Wang, P. X. Lei, W. J. Song, W. H. Ma and J. C. Zhao, *Environ. Sci. Technol.*, 2006, **40**, 3965–3970.
- P. X. Lei, C. C. Chen, J. Yang, W. H. Ma, J. C. Zhao and L. Zang, *Environ. Sci. Technol.*, 2005, **39**, 8466–8474.
- J. H. Li, W. L. Kang, X. Yang, X. D. Yu, L. L. Xu, Y. H. Guo, H. B. Fang and S. D. Zhang, *Desalination*, 2010, **255**, 107–116.
- S. Kim, J. Yeo and W. Choi, *Appl. Catal., B*, 2008, **84**, 148–155.
- N. Lu, Y. H. Zhao, H. B. Liu, Y. H. Guo, X. Yuan, H. Xu, H. F. Peng and H. W. Qin, *J. Hazard. Mater.*, 2011, **199–200**, 1–8; Q. Wang, M. Zhang, C. Chen, W. Ma and J. Zhao, *Angew. Chem., Int. Ed.*, 2010, **49**, 7976–7979.
- M. Huang, X. Han, C. Hung, J. Lin, P. Wu, J. Wu and S. Liu, *J. Catal.*, 2014, **320**, 42–51.

- 33 E. Androulaki, A. Hiskia, D. Dimotikali, C. Minero, P. Calza, E. Pelizzetti and E. Papaconstantinou, *Environ. Sci. Technol.*, 2000, **34**, 2024–2028; J. Yu, G. Dai and B. Cheng, *J. Phys. Chem. C*, 2010, **114**, 19378–19385.
- 34 D. M. Sullivan and M. L. Bruening, *Chem. Mater.*, 2003, **15**, 281–287.
- 35 A. L. Souza, F. G. Tremiliosi, L. T. Kubota, R. K. Mendes, A. M. Botelho do Rego, O. N. Oliveira Jr, C. Henry de Villeneuve, J. N. Chazalviel, P. Allongue, F. Ozanam and U. P. Rodrigues Filho, *RSC Adv.*, 2014, **4**(56), 29612–29621;
- N. Gu, D. Wei, L. Niu and A. Ivaska, *Electrochim. Acta*, 2006, **51**(27), 6038–6044.
- 36 Z. X. Sun, L. Xu, W. H. Guo, B. B. Xu, S. P. Liu and F. Y. Li, *J. Phys. Chem. C*, 2010, **114**, 5211–5216.
- 37 Y. J. Wei, Z. M. Kang and C. G. Liu, *Spectrosc. Spectral Anal.*, 2004, **24**, 1659–1662.
- 38 C. C. Chen, W. Zhao, P. X. Lei, J. C. Zhao and N. Serpone, *Chem.–Eur. J.*, 2004, **10**, 1956–1965.
- 39 A. Mylonas and E. Papaconstantinou, *J. Photochem. Photobiol., A*, 1996, **94**, 77–82; A. Hiskia and E. Papaconstantinou, *Inorg. Chem.*, 1992, **31**, 163–167.